Environmental Science & Technology Letters

pubs.acs.org/journal/estlcu

Letter

Novel Conductive and Redox-Active Molecularly Imprinted Polymer for Direct Quantification of Perfluorooctanoic Acid

Sumbul Hafeez, Aysha Khanam, Han Cao, Brian P. Chaplin, and Wenqing Xu*

Cite This: *Environ. Sci. Technol. Lett.* 2024, 11, 871−877

Read Online

ACCESS | Metrics & More | Article Recommendations | Supporting Information

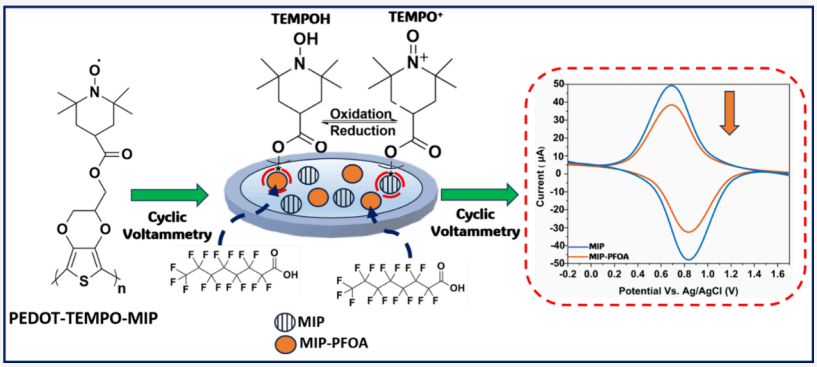

ABSTRACT: This study developed a novel molecularly imprinted polymer (MIP) that is both conductive and redox-active for directly quantifying perfluorooctanoic acid (PFOA) electrochemically. We synthesized the monomer 3,4-ethylenedioxythiophene-2,2,6,6-tetramethylpiperidinyloxy (EDOT-TEMPO) for electropolymerization on a glassy carbon electrode using PFOA as a template, which was abbreviated as PEDOT-TEMPO-MIP. The redox-active MIP eliminated the need for external redox probes. When exposed to PFOA, both anodic and cathodic peaks of MIP showed a decreased current density. This observation can be explained by the formation of a charge-assisted hydrogen bond between the anionic PFOA and MIP's redox-active moieties (TEMPO) that hinder the conversion between the oxidized and reduced forms of TEMPO. The extent of the current density decrease showed excellent linearity with PFOA concentrations, with a method detection limit of 0.28 ng·L^{-1}. PEDOT-TEMPO-MIP also exhibited high selectivity toward PFOA against other per- and polyfluoroalkyl substances (PFAS) at environmentally relevant concentrations. Our results suggest electropolymerization of MIPs was highly reproducible, with a relative standard deviation of 5.1% among three separate MIP electrodes. PEDOT-TEMPO-MIP can also be repeatedly used with good stability and reproducibility for PFOA detection. This study provides an innovative platform for rapid PFAS quantification using redox-active MIPs, laying the groundwork for developing compact PFAS sensors.

KEYWORDS: *per- and polyfluoroalkyl substances (PFAS), perfluorooctanoic acid (PFOA), molecularly imprinted polymer (MIP), electrochemical sensor, conductive polymer, redox-active polymer*

INTRODUCTION

Per- and polyfluoroalkyl substances (PFAS) are a suite of ionizable synthetic organofluorine surfactants widely used in industrial and consumer applications over the past few decades.[1−3] Some PFAS are highly recalcitrant, bioaccumulative, and toxic.[4,5] The U.S. Environmental Protection Agency has set maximum contaminant levels (MCLs) for six PFAS in drinking water, with the MCLs for perfluorooctanesulfonic acid (PFOS) and perfluorooctanoic acid (PFOA) at 4 ng·L^{-1} each as of April 2024.[6] Reports suggest that PFAS are present in the drinking water of 200 million Americans.[7,8] There is consensus that technologies for rapid PFAS detection at sub ng·L^{-1} concentrations are critical but lacking.

The current gold standard of PFAS detection relies on expensive instrumentation (i.e., liquid chromatography-triple quadrupole-tandem mass spectrometry (LC-MS/MS)), which requires specialized operator training and labor-intensive sample processing that takes hours to days, and is cost-prohibitive.[9−12] Consequently, an array of optical and electrochemical PFAS sensors have been developed, but their selectivity remains problematic.[13−16] This aspect is particularly important given that many PFAS exist in mixtures and interfering ions often coexist. Molecularly imprinted polymers (MIPs) offer high selectivity for PFAS due to the molecular

Received: July 9, 2024
Revised: July 30, 2024
Accepted: July 31, 2024
Published: August 5, 2024

"lock-and-key" binding mechanism, which was previously employed for concentrating PFAS from water samples.[17−20] Briefly, MIPs are cross-linked polymers synthesized in the presence of template molecules (e.g., PFAS), which are removed by post-polymerization to create cavities with a size, shape, and binding affinity similar to the template used.[21−23] Combining MIPs with electrochemical detection has gained immense attention, which relies on changes in electrochemical signals upon binding and removal of templates from MIP cavities. MIPs are increasingly used in chemical sensing platforms to detect drug residues,[24,25] organic dyes,[26,27] pesticides,[28,29] pathogens,[21,30] and PFAS.[31−35] However, several major obstacles exist. First, existing MIPs coupled with electrochemical detection are not redox-active and thus require addition and periodic replenishment of external redox probes (e.g., ferric/ferrocyanide), adding complexity to integration and downsizing of sensor systems.[31−33] Moreover, current studies employed non-conductive MIPs (e.g., *o*-phenylenediamine),[31−33,36] limiting electron transfer and signal transduction during measurement. Additionally, several existing conductive MIPs (e.g., polypyrrole and polyaniline) are not sufficiently stable in water, leading to decreased conductivity over time.[37,38]

Herein, we leveraged the high conductivity and robustness of poly-3,4-ethylenedioxythiophene (PEDOT) in water and incorporated 2,2,6,6-tetramethylpiperidinyoxy (TEMPO), a redox-active *N*-oxyl derivative, into PEDOT for direct quantification of PFAS at sub ng·L^{-1} concentrations.[39−43] The detection mechanism for PFOA relies on proton blocking, hindering the conversion of TEMPOH to TEMPO^{+} upon oxidation and reduction (Scheme 1). Specifically, we synthesized and purified the monomer EDOT-TEMPO, performed electropolymerization to obtain PEDOT-TEMPO-MIP using PFOA as a template, established a calibration curve, and assessed the selectivity, stability, and reusability of PEDOT-TEMPO-MIP towards PFOA in the range that is typical in surface water. Our findings provide an innovative platform for rapid ex-situ PFAS quantification by creating a redox-active MIP, eliminating the need for external redox probes, and laying the groundwork for compact PFAS sensor development.

Scheme 1. Proposed Mechanism for Electrochemical Signal Decrease upon the Interaction between PFOA Anion and Redox-Active Moieties on PEDOT-TEMPO-MIP (i.e., TEMPO: TEMPOH/TEMPO^{+}) that Results in Blockage of Conversion between the Oxidized and Reduced Forms of TEMPO

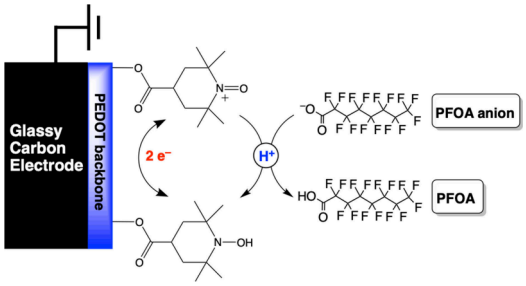

METHODS AND MATERIALS

Chemicals, Material Characterization, and Chemical Analysis. All chemicals, material characterization, and chemical analysis are provided in the Supporting Information (SI) (Texts S1, S2, and S3).

Preparation of MIPs. Details on the preparation of monomer EDOT-TEMPO, PEDOT-TEMPO-MIP, and non-molecularly imprinted PEDOT-TEMPO (PEDOT-TEMPO-NIP) are provided in Text S4.[44,45]

Electrochemical Measurement. All potentials were reported relative to the Ag/AgCl reference electrode. The cyclic voltammetry (CV) scans of glassy carbon electrode, PEDOT-TEMPO-MIP and PEDOT-TEMPO-NIP were collected at a potential range of 0.0−1.5 V with a scan rate of 20 mV·s^{-1} in dichloromethane (DCM) solution containing 0.1 mol·L^{-1} tetrabutylammonium hexafluoro phosphate ($TBAPF_6$) as a commonly used nonaqueous electrolyte. DCM was selected due to its high compatibility with PFOA and $TBAPF_6$ and was used for MIP electropolymerization and electrochemical signal monitoring. By contrast, the rebinding of PFAS was carried out in DI or actual water samples. The direct quantification of PFOA using PEDOT-TEMPO-MIP involves (1) MIP synthesis by electropolymerization in DCM containing $TBAPF_6$, (2) removal of PFOA template with DI, (3) rebinding of PFOA with MIP in DI (or actual water sample), and (4) detection of PFOA captured by MIP in an electrochemical cell containing DCM and $TBAPF_6$. Steps (1) and (4) were performed in an electrochemical cell, and steps (2) and (3) were carried out in batch reactors with water. Furthermore, the reference current density (i_0) was recorded in CV scans in an electrochemical cell in DCM for PEDOT-TEMPO-MIP after template (PFOA) removal. Rebinding of PFOA was conducted by exposing PEDOT-TEMPO-MIP to different PFOA concentrations (i.e., 4.14×10^{-10} to 4.14×10^{-4} g·L^{-1}) in DI water. Afterward, PEDOT-TEMPO-MIP was transferred to an electrochemical cell for CV scans in DCM to investigate the impact of PFOA rebinding on the electrochemical signal. The baseline current density (i_0) of PEDOT-TEMPO-MIP was taken at an anodic peak of TEMPO after PFOA template removal, whereas i was recorded after being exposed to PFOA in DI water (also referred to as "rebinding process"). Three cycles of CV scans were conducted to obtain a stable electrode response (Figure S1). The average value from the second and third scans was used for each measurement. The changes in current density (i.e., $\Delta i = i - i_0$) were plotted against PFOA concentrations for the calibration curve. Each PFOA concentration was measured in triplicate.

RESULT AND DISCUSSION

Characterization of EDOT-TEMPO monomer. The successful synthesis of the EDOT-TEMPO monomer was indicated by its orange crystal (Figure S2) and by ^{1}H nuclear magnetic resonance (NMR) and Fourier transform infrared (FTIR) spectroscopy (Figures S3 and S4). Text S6 explains the NMR and FTIR spectroscopy in detail.

Preparation of PEDOT-TEMPO-MIP and PEDOT-TEMPO-NIP. The CV scans were collected during the electropolymerization of PEDOT-TEMPO-MIP with PFOA (Figure S5). Consistent with the literature,[44,45] we observed a slight shift in the anodic peak of EDOT from 1.2 to 1.4 V and from 0.86 to 0.90 V for TEMPO over ten scans, which was

https://doi.org/10.1021/acs.estlett.4c00557
Environ. Sci. Technol. Lett. 2024, 11, 871−877

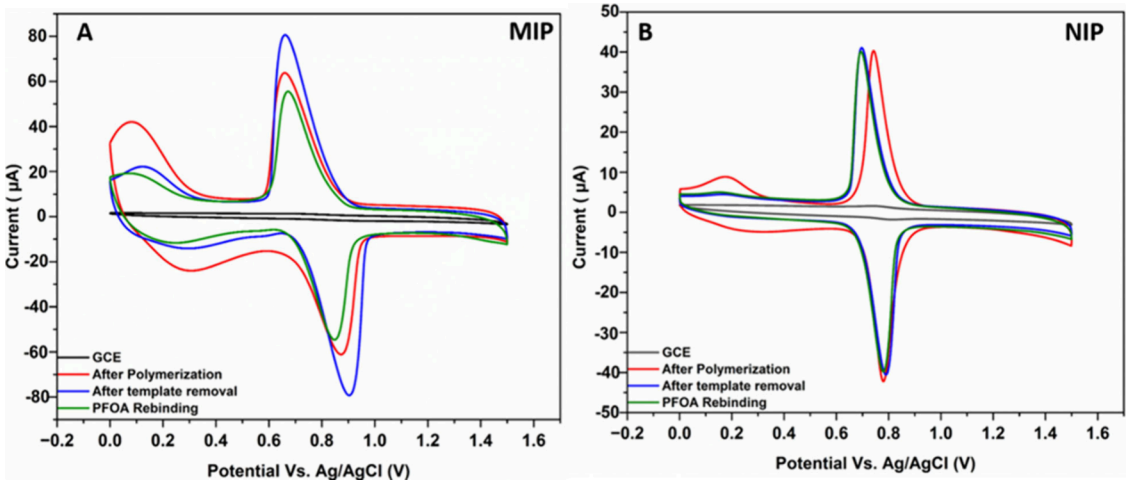

Figure 1. CV scans of bare glassy carbon electrode (black), after electropolymerization (red), after template removal (blue), and after exposure to 4.14×10^{-4} g·L^{-1} PFOA for 30 min (green): (A) PEDOT-TEMPO-MIP and (B) PEDOT-TEMPO-NIP.

attributed to increased resistivity between the working electrode and reference electrode following the growth of PEDOT-TEMPO-MIP film.[44,46] The increased current density following electropolymerization can be explained by increased pseudocapacitance of the film by incorporating more redox-active moieties into the MIP.[44,47] The glassy carbon electrode coated with the PEDOT-TEMPO-MIP shows an apparent blue color (Figure S5).[44,45]

Two characteristic peaks were observed in CV scans of PEDOT-TEMPO-MIP (Figure 1A; red curve): the anodic and cathodic peaks appeared at 0.86 and 0.69 V, respectively, corresponding to the redox-active TEMPO (i.e., TEMPO$^+$, and TEMPOH, Scheme 1).[41−43] The peaks at 0.30 and 0.18 V suggested anodic and cathodic peaks of the PEDOT backbone.[44,45] After electropolymerization, PEDOT-TEMPO-MIP was washed with DI water instead of organic solvent to remove the PFOA template. The rationale of solvent selection was explained in Text S4.[17−19] We observed an increase of 21.1% and 18.5% in current density at anodic and cathodic peaks of PEDOT-TEMPO-MIP, respectively (Figure 1A; blue vs. red curves). When PEDOT-TEMPO-MIP was exposed to 4.14×10^{-4} g·L^{-1} PFOA in DI for 30 min during rebinding, a decrease of 40% and 34% in anodic and cathodic peaks current density was observed, respectively (Figure 1A; green curve). We postulate that the observed decrease in the current density in the presence of PFOA can be attributed to the interaction between the PFOA and TEMPO moieties. Specifically, the anionic PFOA (pK_a = 0.5−3.8)[48,49] may form a charge-assisted hydrogen bond with TEMPOH (pK_a = 5.5−6.2). As a result, the conversion from TEMPOH to TEMPO$^+$ upon oxidation is hindered, causing a decrease in anodic and cathodic peaks' current density (Scheme 1). The formation of a charge-assisted hydrogen bond has been previously reported to form between PFOA and polar groups of various surfaces.[50−52] The closer proximity of pK_a values of two species, the stronger the H-bond formed.[50−52]

PEDOT-TEMPO-NIP was prepared under the same experimental conditions as PEDOT-TEMPO-MIP, but without PFOA. The CV scan for PEDOT-TEMPO-NIP showed CV characteristics similar to those of PEDOT-TEMPO-MIP (Figure 1B; red curve). However, the current density after removing the PFOA template (Figure 1B; blue curve) or rebinding with PFOA for 30 min (Figure 1B; green curve) exhibited negligible changes at both anodic and cathodic peaks of TEMPO, suggesting a lack of PFOA molecular imprinting cavities in PEDOT-TEMPO-NIP.

Electrochemical Measurements of PFOA and Construction of Calibration Curve. To determine the optimal rebinding time for PFOA quantification, we first performed time-dependent rebinding experiments by exposing PEDOT-TEMPO-MIP to four different PFOA concentrations (i.e., 4.14×10^{-10}, 4.14×10^{-9} g·L^{-1}, 4.14×10^{-8} g·L^{-1}, and 4.14×10^{-4} g·L^{-1}). At a higher PFOA concentration (i.e., 4.14×10^{-4} g·L^{-1}), we observed a decrease in current density by 37% to 85% from 30 to 180 min, which plateaued around 240 min (Table S1). The current density decreased to a lesser extent at a lower PFOA concentration (i.e., 4.14×10^{-8} g·L^{-1}, 4.14×10^{-9} g·L^{-1}, 4.14×10^{-10} g·L^{-1}) compared to a higher PFOA concentration (i.e., 4.14×10^{-4} g·L^{-1}), and current density plateaued after 210 min. For consistency, we chose 240 min for all subsequent experiments unless otherwise stated.

The calibration curve of PFOA was constructed by obtaining Δi from the anodic peak of TEMPO after rebinding with PFOA for 5 and 240 min, respectively, at a series of concentrations (i.e., 4.14×10^{-10} g·L^{-1} to 4.14×10^{-4} g·L^{-1}). The rebinding time of 5 min was selected to establish a more realistic scenario for rapid sensing, as shown in Figure 2, Figure S6, and Table S2. The regression analysis indicated a good linear relationship at both rebinding times (5 and 240 min) (i.e., R^2 = 0.98) between Δi and corresponding PFOA concentrations (Figure 2 and Figure S6). A method detection limit (MDL) of 3.26×10^{-9} g·L^{-1} for PEDOT-TEMPO-MIP was determined for 5 min exposure of PFOA using seven replicates of the lowest calibration standard (i.e., 4.14×10^{-9} g·L^{-1}) (Figure 2) following an EPA standard method (Text S5).[53,54] By contrast, a lower MDL of 2.80×10^{-10} g·L^{-1} was achieved for PEDOT-TEMPO-MIP using seven replicates of lowest calibration standard (i.e., 4.14×10^{-10} g·L^{-1}) for 240 min rebinding (Figure S6; Text S5).[53,54] Our results suggest that as PFOA concentrations increase, more PFOA molecules were able to block proton transfer to TEMPO$^+$ moieties, thereby hindering conversion between TEMPO$^+$/TEMPOH and lowering TEMPO anodic peak current density.

Reproducibility, Stability, and Selectivity of PEDOT-TEMPO-MIP. The reusability of PEDOT-TEMPO-MIP was assessed by evaluating the relative change in current density of

https://doi.org/10.1021/acs.estlett.4c00557
Environ. Sci. Technol. Lett. 2024, 11, 871−877

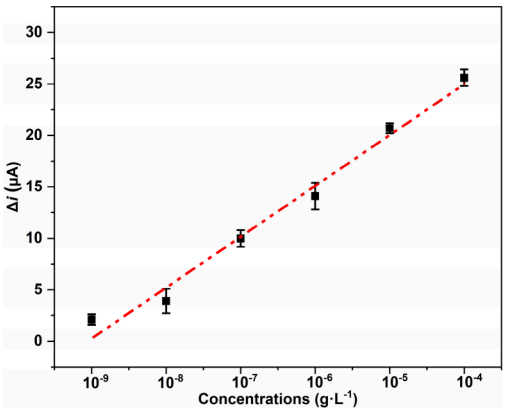

Figure 2. Calibration curve of the current density decrease at the anodic peak of TEMPO (y-axis) vs PFOA concentrations (ranging from 4.14×10^{-9} to 4.14×10^{-4} g·L^{-1}; x-axis). The current density was recorded from the CV scans of PEDOT-TEMPO-MIP after being exposed to PFOA for 5 min. The error bar at each point was derived from triplicate measurements. The linear regression is $y = 4.91x - 4.47$ ($R^2 = 0.98$).

the anodic peak of TEMPO at 0.87 V during five successive measurements of the same PFOA sample (Figure S7). The relative standard deviation (RSD) of five measurements was 6.5%. Although the reference current density (i_0) shifted slightly from −125 to −117 μA, possibly due to some irreversible bindings of PFOA on MIPs, the current density (i) shifted accordingly through consecutive measurements (i.e., from −116 to −108 μA). Our results suggest that PEDOT-TEMPO-MIP can be reused at least five times with good stability and reproducibility. Furthermore, the reproducibility of PEDOT-TEMPO-MIP was demonstrated by measuring 4.14×10^{-9} g L^{-1} PFOA using three different electrodes. The change in current density of the anodic peak of TEMPO at 0.87 V after washing and rebinding with 4.14×10^{-9} g L^{-1} PFOA was observed for each MIP electrode, and values are summarized in Table S3. Our results suggest that electropolymerization of MIPs was highly reproducible with a relative standard deviation (RSD) of 5.1%.

The selectivity of PEDOT-TEMPO-MIP was evaluated by monitoring the current density decrease of anodic peak of TEMPO at 0.87 V when exposed to (i) a single PFOA solution (4.14×10^{-8} g·L^{-1}), (ii) a single non-PFOA solution, namely, perfluorobutanoic acid (PFBA), PFOS, or 6:2 fluorotelomer sulfonamide alkylbetaine (6:2 FTAB) solution (4.14×10^{-8} g·L^{-1}), and (iii) a mixture of PFOA/PFBA, PFOA/PFOS, or PFOA/6:2 FTAB solution (each at 4.14×10^{-8} g·L^{-1}). The current density decreased by 18.4 ± 1.1% when PEDOT-TEMPO-MIP was exposed to single PFOA solution (i.e., 4.14×10^{-8} g·L^{-1}). By contrast, the current density was only reduced by 2.7 ± 0.8%, 1.4 ± 0.6%, and 2.5 ± 0.6% in the presence of a non-template molecule, such as PFBA, PFOS, or 6:2 FTAB solution (i.e., 4.14×10^{-8} g·L^{-1}), respectively, suggesting that none of these compounds was able to effectively block proton transfer and hinder subsequent conversion between TEMPOH and TEMPO$^+$. PEDOT-TEMPO-MIP showed high selectivity toward PFOA against its structural analogs (i.e., PFBA, PFOS, and 6:2 FTAB), which can be explained by the formation of the exact shape and size cavity of template molecule (PFOA) as compared to a non-template molecule with different chain length, headgroup, and charge.[17−19] When PEDOT-TEMPO-MIP was exposed to a mixture of PFOA/PFBA, PFOA/PFOS, and PFOA/6:2 FTAB (each at 4.14×10^{-8} g·L^{-1}), current density decreased by 17.2 ± 3.0%, 14.6 ± 2.8%, and 20.2 ± 3.2%, respectively. Our results from the PFOA mixture system were not significantly different from those of a single PFOA in DI, highlighting the selectivity of MIPs toward PFOA in the presence of its structural analogs.

Lastly, we evaluated the performance of PEDOT-TEMPO-MIP in a surface water sample. The chemical composition and sampling location are provided in Table S4 and Figure S8. Specifically, surface water contains a 7.3 ± 0.4 mg·L^{-1} non-purgeable organic carbon (NPOC) and 7.8 ± 0.1 mg·L^{-1} chloride anion. The absence of PFOA and other PFAS such as PFOS, PFBS, perfluorohexanoic acid (PFHxA), hexafluoropropylene oxide dimer acid (HFPO-DA), and 6:2-fluorotelomersulfonic acid (6:2-FTS) in DI water and collected surface water sample was confirmed by LC-MS/MS. To understand the impact of water matrices on PFOA quantification using PEDOT-TEMPO-MIP, we spiked a known concentration of PFOA (4.14×10^{-8} g·L^{-1}) into the surface water sample. The relative current density change of the anionic peak of TEMPO after rebinding was monitored following the same protocol. We observed a decrease in the current density of MIP (Figure 3)

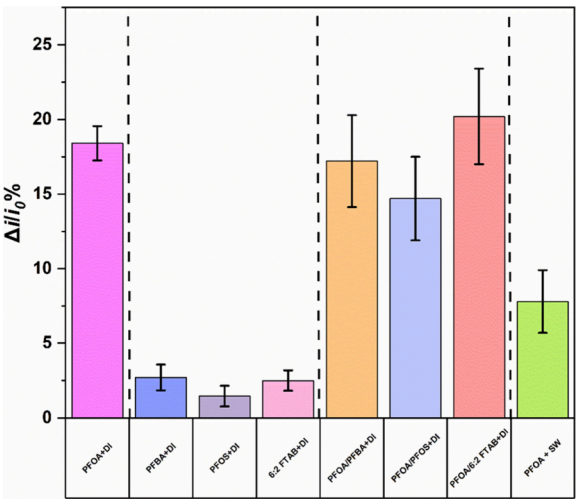

Figure 3. Decrease in current density at the anodic peak of TEMPO of PEDOT-TEMPO-MIP after rebinding with (i) a single PFOA, PFBA, PFOS or 6:2 FTAB (each at 4.14×10^{-8} g·L^{-1}) in DI water, (ii) a mixture of PFOA/PFBA, PFOA/PFOS, or PFOA/6:2 FTAB (each at 4.14×10^{-8} g·L^{-1}) in DI water, and (iii) spiked a known concentration of PFOA (4.14×10^{-8} g·L^{-1}) into the surface water sample for 240 min.

by 7.8 ± 2.1% in a surface water sample, which was 18.4 ± 1.1% lower than when MIP was exposed to the same concentration of PFOA in DI water. The decrease in current density in surface water compared to DI can be attributed to the presence of interfering ions (Cl^-, SO_4^{2-}) that are small enough to occupy MIP cavities but could not hinder H^+ transfer between TEMPOH and TEMPO$^+$ due to the lack of ability to form H-bond.

■ ENVIRONMENTAL SIGNIFICANCE

This work demonstrates the feasibility of synthesizing PEDOT-TEMPO-MIP that can directly quantify sub ng·L^{-1} PFAS concentrations electrochemically without using external redox probes. Specifically, we directly quantify PFOA with

https://doi.org/10.1021/acs.estlett.4c00557
Environ. Sci. Technol. Lett. 2024, 11, 871−877

MIP by utilizing specific interactions between PFOA and binding sites that cause signal reduction. By contrast, past published methods rely on external redox probes, which quantify PFOA indirectly and are more likely to result in a false positive. Our obtained MDL for PEDOT-TEMPO-MIP is significantly lower than reported MDL values from potentiometric, fluorescence, and calorimetric sensors for PFAS (10^{-5} to 10^{-3} g·L^{-1})[55−57] and slightly lower than reported MDLs for photoelectrochemical, electrochemical impedance spectroscopy, and Raman spectroscopy sensors (10^{-9} to 10^{-8} g·L^{-1}).[58−60] It is worth noting that our calculated MDL of PEDOT-TEMPO-MIP may be further improved by applying other electrochemical techniques (e.g., differential pulse voltammetry or square wave voltammetry) to reduce background noise and enhance sensitivity.[31,47]

Moreover, a novel PFAS sensing mechanism was elucidated for the first time. Specifically, we utilized redox-active properties of PEDOT-TEMPO-MIP, namely, the conversion between TEMPOH and TEMPO$^+$ upon oxidation and subsequent reduction, to directly quantify PFAS. The aspect of directly quantifying PFAS is of significance for environmental monitoring. Existing electrochemical detection of PFAS relies on external redox probes (e.g., ferric/ferrocyanide), which must be added and replenished periodically.[31−33] The ability to directly quantify PFAS helps simplify component integration for sensor platforms and enables the development of portable devices. The reversible nature of the redox-active TEMPO also helps eliminate the need for reagent replenishment and lays the groundwork for continuous monitoring, which may revolutionize the field of environmental monitoring.

Lastly, the ability to rapidly quantify PFAS is highly desirable in the field. For instance, current gold-standard LC-MS/MS requires complex sample preparation and analysis protocols, which take hours to days to obtain results.[3,10,12,59] The typical sample preparation and testing time for surface-enhanced raman spectroscopy (SERS) is in the range of hours, which relies on a diffusion-controlled process to accumulate sufficient PFAS between neighboring nanoparticles to reach the best signal enhancement.[61−63] By contrast, PFAS detection in our proposed platform can be accomplished within a few minutes (e.g., 5 min), which lays the groundwork for rapid detection, that is urgently needed in environmental science and engineering. Although some loss of sensitivity was observed due to interfering ions in water matrices, presumably, the calibration curve can be prepared in the same water matrices but at higher concentrations than native water, which might help correct background interference. Nonetheless, our PFAS sensor can serve as a screening tool to quickly identify water bodies impacted by PFAS pollution, allowing further PFAS characterization. Future work on the scale-up feasibility of MIP-coupled electrochemical sensors, cost analysis, and potential for real-time sensing are warranted.

■ ASSOCIATED CONTENT

Supporting Information

The Supporting Information is available free of charge at https://pubs.acs.org/doi/10.1021/acs.estlett.4c00557.

Details of chemical and reagents (Text S1); material characterization (Text S2); chemical analysis (Text S3); preparation of MIPs (Text S4); synthesis and purification of 3,4-ethylenedioxythiophene-2,2,6,6-tetramethylpiperdinyloxy (EDOT-TEMPO) monomer, electrochemical polymerization of poly-3,4-ethylenedioxythiophene-2,2,6,6-tetramethylpiperdinyloxy (PEDOT-TEMPO-MIP) and nonmolecularly imprinted polymers (PEDOT-TEMPO-NIP); method detection limit (MDL) calculation (Text S5); characterization of EDOT-TEMPO monomer (Text S6); scheme for the synthesis of EDOT-TEMPO monomer via the esterification reaction between EDOT-MeOH and TEMPO-COOH at room temperature for 72 h (Scheme S1); scheme for the synthesis of PEDOT-TEMPO-MIP using 1 mmol·L^{-1} EDOT-TEMPO and 1 mmol·L^{-1} PFOA in a 0.1 M $TBAPF_6$ dichloromethane solution, employing a scan rate of 20 mV·s^{-1} and a potential range of 0−1.5 V. (Scheme S2); three cycles of cyclic voltammograms (CV) scans of PEDOT-TEMPO-MIP after template removal in 0.1 M $TBAPF_6$ dichloromethane solution (Figure S1); orange color crystal of EDOT-TEMPO monomer after purification (Figure S2); ^{1}H NMR spectrum of EDOT-TEMPO (Figure S3); FTIR spectrum of EDOT-TEMPO (Figure S4); ten cycles of CV scans during electropolymerization of PEDOT-TEMPO-MIP using EDOT-TEMPO in 0.1 M $TBAPF_6$ dichloromethane solution (Figure S5); the calibration curve of the current density decreases at the anodic peak of TEMPO (y-axis) vs PFOA concentrations ranging from 4.14×10^{-9} to 4.14×10^{-4} g·L^{-1} (x-axis). (Figure S6); the relative changes in the current density of TEMPO's anodic peak at 0.87 V over 5 cycles of washing (template removal) and rebinding (when exposed to 4.14×10^{-9} g·L^{-1} PFOA). (Figure S7); the sampling location of the surface water from a pond near West Windsor Township, New Jersey, USA (Figure S8); the decrease in current density of the anodic peak of TEMPO during PFOA rebinding at different time intervals (Table S1); the decrease in current density of the anodic peak of TEMPO after being exposed to PFOA in a concentration range of 4.14×10^{-4} g·L^{-1} to 4.14×10^{-9} g·L^{-1} for 5 min (Table S2); reproducibility of PFOA (4.14×10^{-9} g L^{-1}) measurements using three PEDOT-TEMPO-MIP electrodes (Table S3) and the chemical composition of the collected surface water sample (Table S4) (PDF)

■ AUTHOR INFORMATION

Corresponding Author

Wenqing Xu − *Department of Civil and Environmental Engineering, Villanova University, Villanova, Pennsylvania 19085, United States;* orcid.org/0000-0002-9838-8220; Email: wenqing.xu@villanova.edu

Authors

Sumbul Hafeez − *Department of Civil and Environmental Engineering, Villanova University, Villanova, Pennsylvania 19085, United States*

Aysha Khanam − *Department of Civil and Environmental Engineering, Villanova University, Villanova, Pennsylvania 19085, United States*

Han Cao − *Department of Civil and Environmental Engineering, Villanova University, Villanova, Pennsylvania 19085, United States;* orcid.org/0000-0002-9451-6926

Brian P. Chaplin − *Department of Chemical Engineering, University of Illinois at Chicago, Chicago, Illinois 60607, United States;* orcid.org/0000-0003-1668-5414

Complete contact information is available at: https://pubs.acs.org/10.1021/acs.estlett.4c00557

Notes

The authors declare no competing financial interest.

■ ACKNOWLEDGMENTS

W.X. and S.H. acknowledge support from the National Institutes of Health award (1R01ES032671-01). W.X. would also like to acknowledge support by the U.S. Department of Defense through the Strategic Environmental Research and Development Program (SERDP ER23-3593).

■ REFERENCES

(1) Ateia, M.; Alsbaiee, A.; Karanfil, T.; Dichtel, W. Efficient PFAS Removal by Amine-Functionalized Sorbents: Critical Review of the Current Literature. *Environ. Sci. Technol. Lett.* **2019**, *6* (12), 688−695.

(2) Xiao, F. Emerging Poly- and Perfluoroalkyl Substances in the Aquatic Environment: A Review of Current Literature. *Water Res.* **2017**, *124* (1), 482−495.

(3) Wang, Y.; Darling, S. B.; Chen, J. Selectivity of Per- And Polyfluoroalkyl Substance Sensors and Sorbents in Water. *ACS Appl. Mater. Interfaces* **2021**, *13* (51), 60789−60814.

(4) Higgins, C. P.; Luthy, R. G. Sorption of Perfluorinated Surfactants on Sediments. *Environ. Sci. Technol.* **2006**, *40* (23), 7251−7256.

(5) Klemes, M. J.; Skala, L. P.; Ateia, M.; Trang, B.; Helbling, D. E.; Dichtel, W. R. Polymerized Molecular Receptors as Adsorbents to Remove Micropollutants from Water. *Acc. Chem. Res.* **2020**, *53* (10), 2314−2324.

(6) U.S. EPA. Drinking Water Health Advisories for polyfluoroalkyl-substances (PFAS). https://www.epa.gov/sdwa/and-polyfluoroalkyl-substances-pfas. https://www.epa.gov/sdwa/and-polyfluoroalkyl-substances-pfas (accessed April 10, 2024).

(7) Rogers, R. D.; Reh, C. M.; Breysse, P. Advancing Per- and Polyfluoroalkyl Substances (PFAS) Research: An Overview of ATSDR and NCEH Activities and Recommendations. *J. Expo. Sci. Environ. Epidemiol.* **2021**, *31* (6), 961−971.

(8) Cousins, I. T.; Dewitt, J. C.; Glüge, J.; Goldenman, G.; Herzke, D.; Lohmann, R.; Ng, C. A.; Scheringer, M.; Wang, Z. The High Persistence of PFAS Is Sufficient for Their Management as a Chemical Class. *Environ. Sci. Process. Impacts* **2020**, *22* (12), 2307−2312.

(9) *Method 533: Determination of Per- and Polyfluoroalkyl Substances in Drinking Water by Isotope Dilution Anion Exchange Solid Phase Extraction and Liquid Chromatography/Tandem Mass Spectrometry*; Doc. No. 815-B-19-020; USEPA, 2019; pp 1−52.

(10) Denly, E.; Morin, K. A Review of Draft Environmental Protection Agency Method 1633: A Data User's Perspective. *Remediation* **2022**, *32* (1−2), 91−95.

(11) Menger, R. F.; Funk, E.; Henry, C. S.; Borch, T. Sensors for Detecting Per- and Polyfluoroalkyl Substances (PFAS): A Critical Review of Development Challenges, Current Sensors, and Commercialization Obstacles. *Chem. Eng. J.* **2021**, *417* (8), No. 129133.

(12) Rehman, A. U.; Crimi, M.; Andreescu, S. Current and Emerging Analytical Techniques for the Determination of PFAS in Environmental Samples. *Trends Environ. Anal. Chem.* **2023**, *37* (8), No. e00198.

(13) Wang, J. Portable Electrochemical Systems. *TrAC - Trends Anal. Chem.* **2002**, *21* (4), 226−232.

(14) Al Amin, M.; Sobhani, Z.; Liu, Y.; Dharmaraja, R.; Chadalavada, S.; Naidu, R.; Chalker, J. M.; Fang, C. Recent Advances in the Analysis of Per- and Polyfluoroalkyl Substances (PFAS)—A Review. *Environ. Technol. Innov.* **2020**, *19*, No. 100879.

(15) Garg, S.; Kumar, P.; Greene, G. W.; Mishra, V.; Avisar, D.; Sharma, R. S.; Dumée, L. F. Nano-Enabled Sensing of per-/Poly-Fluoroalkyl Substances (PFAS) from Aqueous Systems − A Review. *J. Environ. Manage.* **2022**, *308* (1), No. 114655.

(16) Tasfaout, A.; Ibrahim, F.; Morrin, A.; Brisset, H.; Sorrentino, I.; Nanteuil, C.; Laffite, G.; Nicholls, I. A.; Regan, F.; Branger, C. Molecularly Imprinted Polymers for Per- and Polyfluoroalkyl Substances Enrichment and Detection. *Talanta* **2023**, *258* (3), No. 124434.

(17) Yu, Q.; Deng, S.; Yu, G. Selective Removal of Perfluorooctane Sulfonate from Aqueous Solution Using Chitosan-Based Molecularly Imprinted Polymer Adsorbents. *Water Res.* **2008**, *42* (12), 3089−3097.

(18) Cao, F.; Wang, L.; Ren, X.; Sun, H. Synthesis of a Perfluorooctanoic Acid Molecularly Imprinted Polymer for the Selective Removal of Perfluorooctanoic Acid in an Aqueous Environment. *J. Appl. Polym. Sci.* **2016**, *133* (15), 1−10.

(19) Cao, F.; Wang, L.; Tian, Y.; Wu, F.; Deng, C.; Guo, Q.; Sun, H.; Lu, S. Synthesis and Evaluation of Molecularly Imprinted Polymers with Binary Functional Monomers for the Selective Removal of Perfluorooctanesulfonic Acid and Perfluorooctanoic Acid. *J. Chromatogr. A* **2017**, *1516*, 42−53.

(20) Feng, H.; Wang, N.; Tran.T, T.; Yuan, L.; Li, J.; Cai, Q. Surface Molecular Imprinting on Dye-(NH_2)-SiO_2 NPs for Specific Recognition and Direct Fluorescent Quantification of Perfluorooctane Sulfonate. *Sensors and Actuators, B: Chemical.* **2014**, *195* (5), 266−273.

(21) Wang, R.; Wang, L.; Yan, J.; Luan, D.; Sun, T.; Wu, J.; Bian, X. Rapid Sensitive and Label-Free Detection of Pathogenic Bacteria Using a Bacteria-Imprinted Conducting Polymer Film-Based Electrochemical Sensor. *Talanta* **2021**, *226* (1), No. 122135.

(22) Li, G.; Row, K. H. Recent Applications of Molecularly Imprinted Polymers (MIPs) on Micro-Extraction Techniques. *Sep. Purif. Rev.* **2018**, *47* (1), 1−18.

(23) Alizadeh, T.; Ganjali, M. R.; Zare, M.; Norouzi, P. Development of a Voltammetric Sensor Based on a Molecularly Imprinted Polymer (MIP) for Caffeine Measurement. *Electrochim. Acta* **2010**, *55* (5), 1568−1574.

(24) Wang, L.; Pagett, M.; Zhang, W. Molecularly Imprinted Polymer (MIP) Based Electrochemical Sensors and Their Recent Advances in Health Applications. *Sensors Actuators Rep.* **2023**, *5* (2), No. 100153.

(25) Guo, Z.; Xu, W.; Xu, G.; Jia, Q. An Updated Overview of MOF@MIP in Drug Carrier and Drug Analysis: Construction, Application and Prospective. *TrAC - Trends Anal. Chem.* **2023**, *167*, No. 117275.

(26) Lu, Z.; Wei, K.; Ma, H.; Xiong, Q.; Li, Y.; Sun, M.; Wang, X.; Wang, Y.; Wu, C.; Su, G.; Bai, Y.; Deng, R.; Ye, J.; Zhou, C.; Rao, H. Nanoarchitectonics of on−off Ratiometric Signal Amplified Electrochemical Sensor for Chlorpromazine with Molecularly Imprinted Polymer Based on Ni-MOF/Fe-MOF-5 Hybrid Au Nanoparticles. *Sep. Purif. Technol.* **2023**, *327* (5), No. 124858.

(27) Nag, S.; Das, D.; Naskar, H.; Tudu, B.; Bandyopadhyay, R.; Roy, R. B. A Novel Molecular Imprinted Polymethacrylic Acid Decorated Graphite Electrochemical Sensor for Analyzing Metanil Yellow Adulteration in Food. *IEEE Sens. J.* **2023**, *23* (18), 20951−20958.

(28) Atef Abdel Fatah, M.; Abd El-Moghny, M. G.; El-Deab, M. S.; Mohamed El Nashar, R. Application of Molecularly Imprinted Electrochemical Sensor for Trace Analysis of Metribuzin Herbicide in Food Samples. *Food Chem.* **2023**, *404* (3), No. 134708.

(29) Ayivi, R. D.; Obare, S. O.; Wei, J. Molecularly Imprinted Polymers as Chemosensors for Organophosphate Pesticide Detection and Environmental Applications. *TrAC - Trends Anal. Chem.* **2023**, *167* (8), No. 117231.

(30) Zheng, X.; Khaoulani, S.; Ktari, N.; Lo, M.; Khalil, A. M.; Zerrouki, C.; Fourati, N.; Chehimi, M. M. Towards Clean and Safe Water: A Review on the Emerging Role of Imprinted Polymer-based

Electrochemical Sensors. *Sensors* **2021**, *21* (13), 1−42, DOI: 10.3390/s21134300.
(31) Karimian, N.; Stortini, A. M.; Moretto, L. M.; Costantino, C.; Bogialli, S.; Ugo, P. Electrochemosensor for Trace Analysis of Perfluorooctanesulfonate in Water Based on a Molecularly Imprinted Poly(o-Phenylenediamine) Polymer. *ACS Sensors* **2018**, *3* (7), 1291−1298.
(32) Glasscott, M. W.; Vannoy, K. J.; Kazemi, R.; Verber, M. D.; Dick, J. E. μ-MIP: Molecularly Imprinted Polymer-Modified Microelectrodes for the Ultrasensitive Quantification of GenX (HFPO-DA) in River Water. *Environ. Sci. Technol. Lett.* **2020**, *7* (7), 489−495.
(33) Kazemi, R.; Potts, E. I.; Dick, J. E. Quantifying Interferent Effects on Molecularly Imprinted Polymer Sensors for Per- A Nd Polyfluoroalkyl Substances (PFAS). *Anal. Chem.* **2020**, *92* (15), 10597−10605.
(34) Fang, C.; Chen, Z.; Megharaj, M.; Naidu, R. Potentiometric Detection of AFFFs Based on MIP. *Environ. Technol. Innov.* **2016**, *5*, 52−59.
(35) Chen, S.; Li, A.; Zhang, L.; Gong, J. Molecularly Imprinted Ultrathin Graphitic Carbon Nitride Nanosheets-Based Electrochemiluminescence Sensing Probe for Sensitive Detection of Perfluorooctanoic Acid. *Anal. Chim. Acta* **2015**, *896*, 68−77.
(36) Tran.T, T.; Li, J.; Feng, H.; Cai, J.; Yuan, L.; Wang, N.; Cai, Q. Molecularly Imprinted Polymer Modified TiO2 Nanotube Arrays for Photoelectrochemical Determination of Perfluorooctane Sulfonate (PFOS). *Sensors Actuators, B Chem.* **2014**, *190*, 745−751.
(37) Pang, A. L.; Arsad, A.; Ahmadipour, M. Synthesis and Factor Affecting on the Conductivity of Polypyrrole: A Short Review. *Polymers for Advanced Techs* **2021**, *32* (4), 1428−1454.
(38) Liu, Y.; Hwang, B. Mechanism of Conductivity Decay of Polypyrrole Exposed to Water and Enhancement of Conductivity Stability of Copper (I) Modified Polypyrrole. *J. Electroanal. Chem.* **2001**, *501*, 100−106.
(39) Sun, K.; Zhang, S.; Li, P.; Xia, Y.; Zhang, X.; Du, D.; Isikgor, F. H.; Ouyang, J. Review on Application of PEDOTs and PEDOT:PSS in Energy Conversion and Storage Devices. *Journal of Materials Science: Materials in Electronics.* **2015**, *26*, 4438−4462.
(40) Kayser, L. V.; Lipomi, D. J. Stretchable Conductive Polymers and Composites Based on PEDOT and PEDOT: PSS. *Advanced Materials* **2019**, *31*, 1806133.
(41) Wylie, L.; Blesch, T.; Freeman, R.; Hatakeyama-Sato, K.; Oyaizu, K.; Yoshizawa-Fujita, M.; Izgorodina, E. I. Reversible Reduction of the TEMPO Radical: One Step Closer to an All-Organic Redox Flow Battery. *ACS Sustain. Chem. Eng.* **2020**, *8* (49), 17988−17996.
(42) Prakash, N.; Rajeev, R.; John, A.; Vijayan, A.; George, L.; Varghese, A. 2,2,6,6-Tetramethylpiperidinyloxyl (TEMPO) Radical Mediated Electro-Oxidation Reactions: A Review. *ChemistrySelect* **2021**, *6* (30), 7691−7710.
(43) Hickey, D. P.; Schiedler, D. A.; Matanovic, I.; Doan, P. V.; Atanassov, P.; Minteer, S. D.; Sigman, M. S. Predicting Electrocatalytic Properties: Modeling Structure-Activity Relationships of Nitroxyl Radicals. *J. Am. Chem. Soc.* **2015**, *137* (51), 16179−16186.
(44) Casado, N.; Hernández, G.; Veloso, A.; Devaraj, S.; Mecerreyes, D.; Armand, M. PEDOT Radical Polymer with Synergetic Redox and Electrical Properties. *ACS Macro Lett.* **2016**, *5* (1), 59−64.
(45) Schwartz, P. O.; Pejic, M.; Wachtler, M.; Bäuerle, P. Synthesis and Characterization of Electroactive PEDOT-TEMPO Polymers as Potential Cathode Materials in Rechargeable Batteries. *Synth. Met.* **2018**, *243* (4), 51−57.
(46) Elgrishi, N.; Rountree, K. J.; McCarthy, B. D.; Rountree, E. S.; Eisenhart, T. T.; Dempsey, J. L. A Practical Beginner's Guide to Cyclic Voltammetry. *J. Chem. Educ.* **2018**, *95* (2), 197−206.
(47) Cao, H.; Pavitt, A. S.; Hudson, J. M.; Tratnyek, P. G.; Xu, W. Electron Exchange Capacity of Pyrogenic Dissolved Organic Matter (PyDOM): Complementarity of Square-Wave Voltammetry in DMSO and Mediated Chronoamperometry in Water. *Environ. Sci. Process. Impacts* **2023**, *25* (4), 767−780.
(48) Goss, K. U. The pKa values of PFOA and other highly fluorinated carboxylic acids.". *Environ. Sci. Technol.* **2008**, *42* (2), 456−458.
(49) Burns, D. C.; Ellis, D. A.; Li, H.; McMurdo, C. J.; Webster, E. Experimental pKa determination for perfluorooctanoic acid (PFOA) and the potential impact of pKa concentration dependence on laboratory-measured partitioning phenomena and environmental modeling. *Environ. Sci. Technol.* **2008**, *42* (24), 9283−9288.
(50) Xiao, F.; Pignatello, J. J. Effects of post-pyrolysis air oxidation of biomass chars on adsorption of neutral and ionizable compounds. *Environ. Sci. Technol.* **2016**, *50* (12), 6276−6283.
(51) Ni, J.; Pignatello, J. J. Charge-assisted hydrogen bonding as a cohesive force in soil organic matter: water solubility enhancement by addition of simple carboxylic acids. *Environmental Science: Processes & Impacts* **2018**, *20* (9), 1225−1233.
(52) Samonte, P. R. V.; Li, Z.; Mao, J.; Chaplin, B. P.; Xu, W. Pyrogenic carbon-promoted haloacetic acid decarboxylation to trihalomethanes in drinking water. *Water research* **2022**, *210*, 117988.
(53) *Definition and Procedure for the Determination of the Method Detection Limit—Revision 1.11.*; Epa 821-R-16-006; U.S. EPA, 2016, December, pp 1−8.
(54) Li, Z.; Chen, T.; Cui, F.; Xie, Y.; Xu, W. Impact of Chitosan and Polyacrylamide on Formation of Carbonaceous and Nitrogenous Disinfection By-Products. *Chemosphere* **2017**, *178*, 26−33.
(55) Park, H.; Park, J.; Kim, W.; Kim, W.; Park, J. Ultra-Sensitive SERS Detection of Perfluorooctanoic Acid Based on Self-Assembled p-Phenylenediamine Nanoparticle Complex. *J. Hazard. Mater.* **2023**, *453*, No. 131384.
(56) Fang, C.; Zhang, X.; Dong, Z.; Wang, L.; Megharaj, M.; Naidu, R. Smartphone App-Based/Portable Sensor for the Detection of Fluoro-Surfactant PFOA. *Chemosphere* **2018**, *191*, 381−388.
(57) Walekar, L. S.; Zheng, M.; Zheng, L.; Long, M. Selenium and Nitrogen Co-Doped Carbon Quantum Dots as a Fluorescent Probe for Perfluorooctanoic Acid. *Microchim. Acta* **2019**, *186* (5), 1−13.
(58) Fang, C.; Megharaj, M.; Naidu, R. Surface-Enhanced Raman Scattering (SERS) Detection of Fluorosurfactants in Firefighting Foams. *RSC Adv.* **2016**, *6* (14), 11140−11145.
(59) Moro, G.; Cristofori, D.; Bottari, F.; Cattaruzza, E.; De Wael, K.; Moretto, L. M. Redesigning an Electrochemical MIP Sensor for PFOS: Practicalities and Pitfalls. *Sensors* **2019**, *19* (20), 4433.
(60) Gong, J.; Fang, T.; Peng, D.; Li, A.; Zhang, L. A Highly Sensitive Photoelectrochemical Detection of Perfluorooctanic Acid with Molecularly Imprined Polymer-Functionalized Nanoarchitectured Hybrid of AgI-BiOI Composite. *Biosens. Bioelectron.* **2015**, *73*, 256−263.
(61) Rodriguez, K. L.; Hwang, J. H.; Esfahani, A. R.; Sadmani, A. H. M. A.; Lee, W. H. Recent Developments of PFAS-Detecting Sensors and Future Direction: A Review. *Micromachines* **2020**, *11* (7), 667.
(62) Feng, Y.; Dai, J.; Wang, C.; Zhou, H.; Li, J.; Ni, G.; Zhang, M.; Huang, Y. Ag Nanoparticle/Au@Ag Nanorod Sandwich Structures for SERS-Based Detection of Perfluoroalkyl Substances. *ACS Appl. Nano Mater.* **2023**, *6* (15), 13974−13983.
(63) Mcdonnell, C.; Albarghouthi, F. M.; Selhorst, R.; Kelley-Loughnane, N.; Franklin, A. D.; Rao, R. Aerosol Jet Printed Surface-Enhanced Raman Substrates: Application for High-Sensitivity Detection of Perfluoroalkyl Substances. *ACS Omega* **2023**, *8* (1), 1597−1605.